

Two types of surface states in topological crystalline insulators

Junwei Liu,^{1,2} Wenhui Duan,¹ and Liang Fu^{2,*}

¹*Department of Physics and State Key Laboratory of Low-Dimensional Quantum Physics, Tsinghua University, Beijing 100084, People's Republic of China*

²*Department of Physics, Massachusetts Institute of Technology, Cambridge, Massachusetts 02139, USA*

(Received 7 April 2013; published 11 December 2013)

Topological crystalline insulators (TCIs) are new states of matter whose topological distinction relies on the crystal symmetry of periodic solids. The first material realization of TCIs has recently been predicted and observed in IV-VI semiconductor SnTe and related alloys. By combining $k \cdot p$ theory and band structure calculation, we present a unified approach to study topological surface states on various crystal surfaces of these TCI materials based on the electronic structure of the bulk. Depending on the surface orientation, we find two types of surface states with qualitatively different properties. In particular, the (111) surface states consist of four Dirac cones centered at $\bar{\Gamma}$ and \bar{M} , while Dirac cones on (001) and (110) surfaces are located at non-time-reversal-invariant momenta. The latter types of surface states exhibit a Lifshitz transition as a function of Fermi energy, which is accompanied by a Van Hove singularity in the density of states arising from saddle points in the band structure.

DOI: [10.1103/PhysRevB.88.241303](https://doi.org/10.1103/PhysRevB.88.241303)

PACS number(s): 73.20.-r, 73.43.-f, 73.61.Le

Structure and symmetry play an important role in shaping the electronic properties of periodic solids. It is a common phenomenon that materials made of chemically similar elements arranged in the same crystal structure, such as diamond and silicon, often have qualitatively similar electronic properties. Such an empirical relationship between structure and property arises from the fact that the essential electronic properties of many solids are understandable in terms of orbitals and bonds, the characteristics of which depend mostly on crystal structure. For example, both diamond and silicon possess sp^3 hybridized orbitals in a tetrahedral structure. On the other hand, the quantum theory of solids is based on itinerant Bloch waves that form energy bands in momentum space. The global structure of band theory has an interesting consequence: There exist unconventional energy bands that are fundamentally different from a Slater determinant of atomic orbitals. Instead, these “nontrivial” band structures are characterized by topological quantum numbers, and give rise to topological states of matter such as quantum Hall insulators¹ and topological insulators.²⁻⁴

The topological aspect of the band structure implies the inadequacy of the empirical structure-property relation. As a proof of principle, we demonstrated theoretically that for a given crystal structure, there may exist distinct classes of band structures that cannot be adiabatically connected to each other while preserving the symmetry of the crystal.⁵ Those band structures that cannot be deformed to the atomic limit are topologically nontrivial and thus define a new category of topological states, dubbed topological crystalline insulators (TCIs). A hallmark of TCIs is the existence of gapless surface states on crystal faces that preserve the underlying symmetry.^{5,6}

The first material realization of TCI was recently predicted in IV-VI semiconductors SnTe and related alloys $\text{Pb}_x\text{Sn}_{1-x}(\text{Te}, \text{Se})$.⁷ Here the nontrivial topology relies on the presence of reflection symmetry of the rocksalt crystal structure with respect to the (110) mirror plane (and its symmetry-related ones), and is mathematically characterized by an integer topological invariant—the mirror Chern number.⁸ A consequence of topology is that these IV-VI

semiconductors are predicted to possess topological surface states with novel dispersions on a variety of crystal surfaces such as (001), (111), and (110), which are normal to at least one such mirror plane. The (001) surface states have been subsequently observed in angle-resolved photoemission spectroscopy (ARPES) experiments on SnTe,⁹ $\text{Pb}_{1-x}\text{Sn}_x\text{Se}$,¹⁰ and $\text{Pb}_x\text{Sn}_{1-x}\text{Te}$.¹¹ In addition, the spin texture observed in spin-resolved ARPES^{11,12} provides a direct spectroscopic measurement of the mirror Chern number.^{13,14}

The materialization of TCI opens up a new venue for topological phases in a much larger number of material classes than previously thought,¹⁵⁻¹⁹ thereby triggering intensive activities.²⁰⁻²³ From a material viewpoint, IV-VI semiconductors exhibit a wide range of electronic properties (e.g., magnetism, ferroelectricity, and superconductivity) that can be easily tuned by alloying, doping, and strain.²⁴ The technology for synthesizing and engineering these materials, in both bulk and low-dimensional form, has been well developed by decades of efforts.²⁵ Therefore we anticipate that TCIs in IV-VI semiconductors will become an extremely versatile platform for exploring topological quantum phenomena, and, possibly, novel device applications.

In this Rapid Communication, we combine $k \cdot p$ theory and band structure calculation to study TCI surface states on various crystal surfaces of IV-VI semiconductors. We find that the low-energy properties of these surface states are determined by the surface orientation, and can be classified into two types. The (111) surface states consist of four Dirac cones centered at time-reversal-invariant momenta $\bar{\Gamma}$ and \bar{M} ,²⁶ while the (001) and (110) surface states consist of Dirac cones at non-time-reversal-invariant momenta. These low-energy Dirac cones can be regarded as the descendents of two parent Dirac points located close to the bulk conduction and valence band edges, respectively. The presence of two generations of Dirac fermions on the (001) and (110) surface states results in a Lifshitz transition as a function of Fermi energy. This transition is accompanied by a Van Hove singularity in the density of states arising from saddle points in the surface band structure, which is a theoretical prediction of this work. These

results provide a basis for further studies on TCI surface states. Moreover, by deriving the $k \cdot p$ Hamiltonian for surface states from the electronic structure of the bulk, our work provides a *microscopic* understanding of bulk-boundary correspondence in TCI.

We begin by reviewing the band structure of TCIs in the bulk, from which surface states are derived. The band gap of IV-VI semiconductors is located at four L points. For the ionic insulator PbTe, the Bloch state of the valence band at L is derived from the p orbitals of the anion Te, and that of the conduction band from the cation Pb. In contrast, SnTe has an inherently inverted band ordering, in which the valence band is derived from the cation Sn and the conduction band from Te. This band inversion relative to a trivial ionic insulator gives rise to the TCI phase in SnTe.⁷ The band structure near each L point can be described by a four-band $k \cdot p$ theory in the basis of the four Bloch states at L , $\psi_{\sigma,s}(L)$, where $\sigma = 1(-1)$ refers to the state derived from the cation (anion), and s labels the Kramers doublet. The $k \cdot p$ Hamiltonian $H(\mathbf{k})$ is given by (see Ref. 7, and references therein)

$$H(\mathbf{k}) = m_0\sigma_z + v\sigma_x(k_1s_2 - k_2s_1) + v'k_3\sigma_y, \quad (1)$$

where k_3 is along the ΓL direction, and k_1 is along the $(1\bar{1}0)$ axis of reflection. $\vec{\sigma}$ and \vec{s} are two sets of Pauli matrices. The sign of m_0 in (1) captures the two types of band ordering: In our convention $m_0 > 0$ for PbTe and $m_0 < 0$ for SnTe.

The electronic structures of TCI surface states depend crucially on the crystal face orientations. We distinguish two types of crystal surfaces of the rocksalt lattice. For the type-I surface, all four L points are projected to different time-reversal-invariant momenta in the surface Brillouin zone. This is the case for the (111) surface, for which L_1 is projected to $\bar{\Gamma}$ and (L_2, L_3, L_4) are projected to three \bar{M} points. For the type-II surface, different L points are projected to the same surface momenta. This is the case for the (001) surface for which $(L_1, L_2) \rightarrow \bar{X}_1$ and $(L_3, L_4) \rightarrow \bar{X}_2$, as well as the (110) surface for which $(L_1, L_2) \rightarrow \bar{X}$ and $(L_3, L_4) \rightarrow \bar{R}$. The projection from the bulk to surface Brillouin zone is shown in Fig. 1.

(111) surface. The type-I surface states can be obtained straightforwardly by solving the continuum $k \cdot p$ Hamiltonian (1). Following the spirit of Ref. 27, we model the vacuum as a trivial insulator (such as PbTe) with an infinite gap $m_0 = M > 0$, where $M \rightarrow +\infty$. Surface states can now be obtained by solving a domain wall problem in which the Dirac mass m_0 is spatially varying and changes sign across the interface between the TCI and the vacuum. It is well known from field theory that two-dimensional (2D) massless Dirac fermions form at such an interface.^{28–30} Due to the presence of four L valleys, surface states consist of four copies of such Dirac fermions. These four Dirac fermions are located at four *distinct* 2D momenta that correspond to the projection of the four L points onto the type-I surface. Because of their different in-plane momenta, the four L valleys cannot couple with each other as long as in-plane translation symmetry is present, and therefore independently give birth to four branches of Dirac surface states.

A prime example of the type-I surface is (111). It follows from the above analysis that the (111) surface states consist of four Dirac cones: one at $\bar{\Gamma}$, and three others at \bar{M} . The

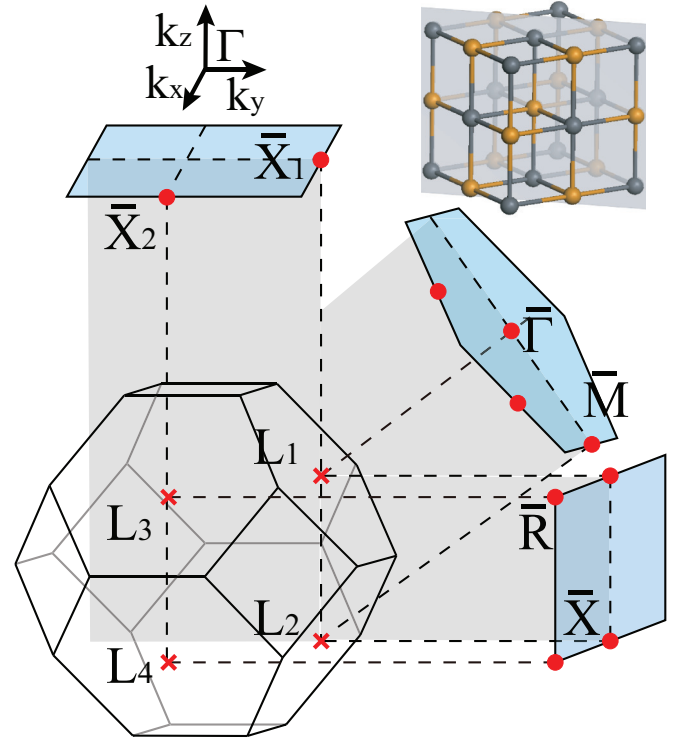


FIG. 1. (Color online) Bulk Brillouin zone of a rocksalt structure and its projection to (001), (111), and (110) surface Brillouin zones. For the (001) surface, L_1 and L_2 are both projected to \bar{X}_1 , and L_3 and L_4 are projected to \bar{X}_2 ; for the (111) surface, L_1 is projected to $\bar{\Gamma}$ and the other three L points are projected to \bar{M} points; for the (110) direction, L_1 and L_2 are projected to \bar{X} and L_3 and L_4 are projected to \bar{R} . The shaded plane passing through Γ , L_1 , and L_2 in the 3D Brillouin zone is invariant under reflection about the $(1\bar{1}0)$ plane in real space.

$k \cdot p$ Hamiltonians at $\bar{\Gamma}$ and \bar{M} are given by $H_{\bar{\Gamma}}(\mathbf{k}) = v(k_1s_2 - k_2s_1)$ and $H_{\bar{M}}(\mathbf{k}) = v_1k_1s_2 - v_2k_2s_1$, where k_1 is along the $\bar{\Gamma}\bar{K}$ direction, and k_2 is along the mirror-invariant $\bar{\Gamma}\bar{M}$ direction.

The presence of these Dirac pockets is confirmed by our band structure calculations on SnTe, based on the tight-binding model³¹ (see Fig. 2). Similar results are obtained for related TCI $\text{Pb}_{1-x}\text{Sn}_x\text{Se}$.³² The Dirac points are found to lie close to the top (bottom) of the valence (conduction) band for Sn (Te) termination. Such surface states are qualitatively similar to interface states between PbTe and SnTe studied in early

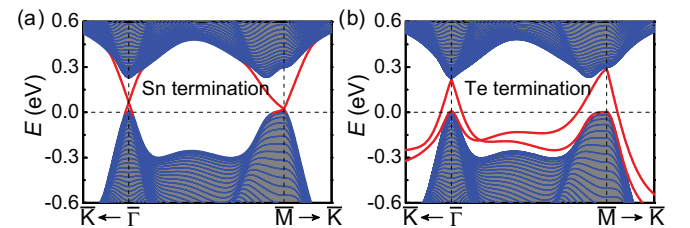


FIG. 2. (Color online) Band structure of the (111) surface for Sn and Te termination. Four Dirac pockets are present: one at $\bar{\Gamma}$ and three at \bar{M} . This leads to two counterpropagating states with opposite mirror eigenvalues on $\bar{\Gamma}\bar{M}$, as predicted from the mirror Chern number $n_M = -2$ in the TCI phase (Ref. 7).

theoretical works.^{28–30} The discovery of TCIs has revealed that such interface states are topologically equivalent to surface states of SnTe, but not PbTe. Moreover, their robust existence has a topological origin that relies on the presence of the (110) mirror symmetry. This symmetry protection can be understood from the two branches of counterpropagating surface states on the mirror-invariant line $\bar{\Gamma}\bar{M}$. They carry opposite mirror eigenvalues and therefore cannot hybridize with each other to open up a gap, in agreement with the prediction based on the mirror Chern number.⁷

(001) surface. The type-II surfaces are much more interesting. In this case, two L points are projected to the same momentum in the surface Brillouin zone. As a result, they interact with each other to create different types of topological surface states with an unusual band dispersion and spin texture. The interaction between the L valleys arises from the physics at the lattice scale, which is not captured by the previous field-theoretic approach.^{28–30}

To correctly obtain the band structure of type-II surfaces, we proceed in two steps. First, we study a hypothetical smooth interface between the TCI and a trivial insulator, in which the Dirac mass is slowly varying in space and gradually changes sign over many lattice constants across the interface. In this smooth limit, scattering between the two L valleys projected to the same in-plane momentum, which requires a large-momentum transfer in the direction normal to the interface, is fully suppressed. We are then justified to use the continuum field theory to solve the domain wall problem for each valley independently and derive an effective Hamiltonian for the resulting multicomponent interface states. Next, imagine deforming the smooth interface into the atomically sharp surface to adiabatically connect interface states to the desired surface states. This deformation procedure introduces intervalley scattering processes at the lattice scale, which are represented by additional terms in the effective Hamiltonian for the surface. Such terms must satisfy all the symmetry of the crystal surface, and therefore can be enumerated by a symmetry analysis. By incorporating these terms into the surface Hamiltonian derived in the previous step, we obtain the final $k \cdot p$ theory for type-II surface states.

We now apply this approach to study the (001) surface. Starting from a smooth interface, we find two coexisting massless Dirac fermions at \bar{X}_1 arising from the L_1 and L_2

valley, respectively, and likewise for the symmetry-related point \bar{X}_2 . These two flavors of Dirac fermions have identical energy-momentum dispersions, resulting in a twofold degeneracy at every \mathbf{k} . The $k \cdot p$ Hamiltonian for this smooth interface is given by $H_{\bar{X}_1}^0(\mathbf{k}) = (v_x k_x s_y - v_y k_y s_x) \otimes I$, where the momentum (k_x, k_y) is measured from \bar{X}_1 , with k_x parallel to $\bar{\Gamma}\bar{X}_2$ and k_y parallel to $\bar{\Gamma}\bar{X}_1$. Here I is identity operator in the flavor space, and \vec{s} is a set of Pauli matrices associated with the two spin components (i.e., Kramers doublet) of each flavor. The velocities in x and y directions are generically different.

Next, we perform a symmetry analysis to deduce the form of those additional terms associated with the physics at the lattice scale, which need to be added to $H_{\bar{X}_1}^0(\mathbf{k})$. Note that \bar{X} is invariant under three point group operations: (i) $x \rightarrow -x$ reflection (M_x); (ii) $y \rightarrow -y$ reflection (M_y); and (iii) twofold rotation around surface normal (C_2). These symmetry operations, plus time-reversal transformation Θ , are represented by the following unitary operators in our $k \cdot p$ theory:

$$\begin{aligned} M_x &: -i s_x, \\ M_y &: -i \tau_x s_y, \\ C_2 &: -i \tau_x s_z, \\ \Theta &: i s_y K. \end{aligned} \quad (2)$$

Importantly, M_x preserves the L_1 and L_2 valley in the bulk and only acts on the electron's spin, whereas both M_y and C_2 interchange L_1 and L_2 and hence involve a flavor-changing operator τ_x . To zeroth order in \mathbf{k} , we find two symmetry-allowed operators, τ_x and $\tau_y s_x$. Therefore our $k \cdot p$ Hamiltonian for the (001) surface states is given by

$$H_{\bar{X}_1}(\mathbf{k}) = (v_x k_x s_y - v_y k_y s_x) + m \tau_x + \delta s_x \tau_y. \quad (3)$$

Note that the two additional terms, parametrized by m and δ , are off diagonal in flavor space, which correctly describe intervalley scattering at the lattice scale.

The $k \cdot p$ Hamiltonian (3) is a main result of this Rapid Communication. We now show that $H_{\bar{X}_1}(\mathbf{k})$ captures all the essential features of type-II surface states. By diagonalizing $H_{\bar{X}_1}(\mathbf{k})$, we obtain four surface bands with energy-momentum dispersions $E_H(\mathbf{k})$, $-E_H(\mathbf{k})$, $E_L(\mathbf{k})$, and $-E_L(\mathbf{k})$, respectively, where $E_{H,L}(\mathbf{k})$ is given by

$$E_{H,L}(\mathbf{k}) = \sqrt{m^2 + \delta^2 + v_x^2 k_x^2 + v_y^2 k_y^2} \pm 2\sqrt{m^2 v_x^2 k_x^2 + (m^2 + \delta^2) k_y^2 v_y^2}. \quad (4)$$

The corresponding surface band structure is plotted in Fig. 3. Two high-energy bands $\pm E_H$ start from energy $E^X \equiv \sqrt{m^2 + \delta^2}$ at \bar{X} and coexist in energy with bulk bands, whereas two low-energy bands $\pm E_L$ lie inside the band gap.

The two terms m and δ arising from the lattice scale play a key role in forming the (001) surface band structure shown in Fig. 3. To start with, a finite m turns the two flavors of massless Dirac fermions into “bonding” ($\tau_x = 1$) and “antibonding” ($\tau_x = -1$) Dirac cones, which are centered at \bar{X} and have

energy $\pm m$ that is close to the bulk conduction and valence band edges, respectively. If δ were zero, the lower band of the upper Dirac cone and the upper band of the lower Dirac cone would cross each other at $E = 0$ over an elliptical contour C enclosing \bar{X} , defined by $v_x^2 k_x^2 + v_y^2 k_y^2 = m^2$. However, a nonzero δ turns this band crossing into an anticrossing via hybridization. Importantly, the hybridization matrix element depends on the direction of \mathbf{k} , and leads to a p -wave hybridization gap: $\Delta(\mathbf{k}) = 2\delta \cdot v_x k_x / m$, $\mathbf{k} \in C$. The

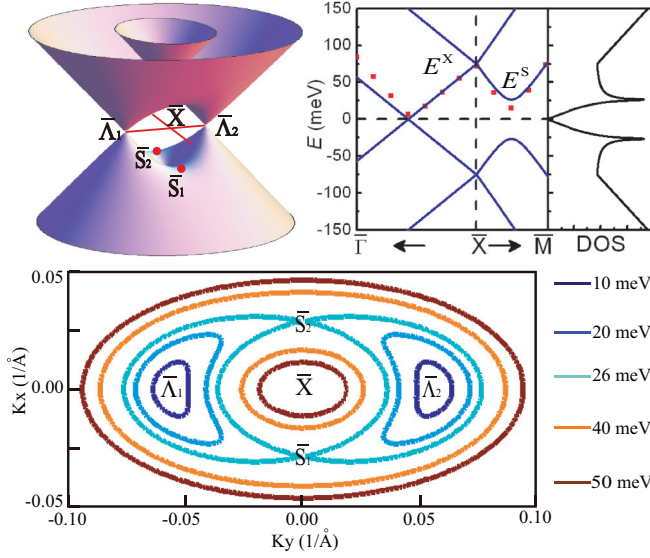


FIG. 3. (Color online) $k \cdot p$ band structure for the (001) surface states. A pair of low-energy Dirac cones, located at $\bar{\Lambda}_1$ and $\bar{\Lambda}_2$ on the line $\bar{X}\bar{\Gamma}$, is formed by the interaction between two high-energy Dirac bands centered at \bar{X} . $k \cdot p$ parameters are obtained by fitting with *ab initio* results (shown by red dots) on SnTe taken from Ref. 7: $v_x = 2.4 \text{ eV \AA}$, $v_y = 1.3 \text{ eV \AA}$, $m = 70 \text{ meV}$, and $\delta = 26 \text{ meV}$. The constant-energy contour evolves rapidly with increasing energy from the Dirac point, changing from two disconnected electron pockets to a large electron pocket and a small hole pocket via a Lifshitz transition. At this transition point, a saddle point \bar{S} on the line $\bar{X}\bar{M}$ leads to a Van Hove singularity in density of states at energy $E^S = \delta$.

fact that $\Delta(\mathbf{k})$ vanishes along the mirror-symmetric line $\bar{\Gamma}\bar{X}_1$ is a consequence of the unique electronic topology of the TCI protected by mirror symmetry. As can be seen from (2) and (3), the two low-energy bands $\pm E_L$ have *opposite* M_x mirror eigenvalues on the k_y line $\bar{X}_1\bar{\Gamma}$, but *identical* M_y mirror eigenvalues on the k_x line $\bar{X}_1\bar{M}$. As a result, hybridization is strictly forbidden on $\bar{X}_1\bar{\Gamma}$, but allowed on $\bar{X}_1\bar{M}$. The presence of such a protected band crossing on $\bar{X}_1\bar{\Gamma}$, but not elsewhere, leads to a pair of zero-energy Dirac points $\bar{\Lambda}_{1,2}$ located symmetrically away from \bar{X}_1 at momenta $\bar{\Lambda}_{1,2} = (0, \pm\sqrt{m^2 + \delta^2}/v_y)$. By linearizing the band structure near each $\bar{\Lambda}$, we obtain the two-component massless Dirac fermion at low energy⁷

$$H_{\bar{\Lambda}_1}(\delta\mathbf{k}) = \tilde{v}_x \delta k_x \sigma_y - v_y \delta k_y \sigma_x, \quad (5)$$

where $\delta\mathbf{k} \equiv \mathbf{k} - \bar{\Lambda}_1$ and the Dirac velocity along $\bar{\Gamma}\bar{X}_1$ is reduced from v_x : $\tilde{v}_x = v_x \delta / \sqrt{m^2 + \delta^2}$.

Our $k \cdot p$ theory thus demonstrates how these low-energy Dirac cones in type-II surfaces are derived from parent Dirac fermions at high energy. By doing so, it also captures essential high-energy features of the (001) surface states that are previously found in *ab initio* calculations.⁷ As shown in Fig. 3, the band dispersion and constant energy contours evolve rapidly and undergo a change in topology (i.e., Lifshitz transition) with increasing energy away from the Dirac point. For $|E| < \delta$, the Fermi surface consists of two disconnected Dirac pockets outside \bar{X} . At $|E| = \delta$, the two pockets touch each other at two saddle points \bar{S}_1 and \bar{S}_2 located at the

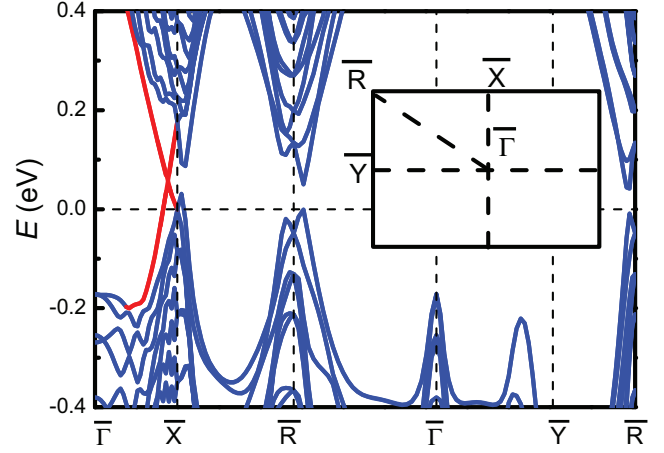


FIG. 4. (Color online) Band structure of the SnTe (110) surface, from our *ab initio* calculations. The inset shows the surface Brillouin zone. A pair of Dirac cones is present on the line $\bar{X}\bar{\Gamma}\bar{X}$, but absent along other high-symmetry lines.

momentum $(\pm m/v_x, 0)$, resulting in a Van Hove singularity in the density of states, shown in Fig. 3. The effective mass tensor at the saddle point is given by $m_{xx} = \delta/v_x^2$ and $m_{yy} = -m^2/(\delta \cdot v_y^2)$. For $|E| > \delta$, the Fermi surface changes into two pockets of different carrier types, both centered at \bar{X} .

As shown in Fig. 3, our $k \cdot p$ band structure (4) fits well with the previous *ab initio* calculation of the SnTe (001) surface in a wide energy range.⁷ Further improvement can be made by incorporating additional intervalley terms that are linear in \mathbf{k} into our $k \cdot p$ Hamiltonian (4). This leads to a sophisticated $k \cdot p$ theory with seven independent parameters, which is closely related to a recent study by Fang *et al.*³⁷ Since these additional terms do not affect any essential aspect of the (001) surface band structure, they are not considered in the main text.³⁸

(110) surface. We end by briefly discussing another type-II surface, (110). In this case, L_1 and L_2 are projected to \bar{X} , and L_3 and L_4 are projected to \bar{R} . Bulk-boundary correspondence based on the electronic topology of TCIs predicts the existence of a pair of counterpropagating states with opposite mirror eigenvalues on $\bar{\Gamma}\bar{X}$.⁷ This is confirmed by our *ab initio* calculation³³ for SnTe (110) shown in Fig. 4: A pair of Dirac cones is found on the line $\bar{X}\bar{\Gamma}\bar{X}$, but not along other high-symmetry lines. Since \bar{X} on the (110) surface has the same symmetry as \bar{X}_1 on the (001) surface including two mirror planes plus a twofold axis, our $k \cdot p$ theory (2) and (3) applies equally well to the (110) surface band structure near \bar{X} .

Note added: Recently, we learned of a related work on the (001) surface states of TCI.³⁹

We thank Timothy Hsieh and Hsin Lin for helpful discussions and related collaborations. This work is supported partly by the DOE Office of Basic Energy Sciences, Division of Materials Sciences and Engineering under Award No. DE-SC0010526. J.L. and W.D. acknowledge the support of the Ministry of Science and Technology of China (Grants No. 2011CB921901 and No. 2011CB606405), and the National Natural Science Foundation of China (Grant No. 11074139).

*Corresponding author: liangfu@mit.edu

- ¹F. D. M. Haldane, *Phys. Rev. Lett.* **61**, 2015 (1988).
- ²M. Z. Hasan and C. L. Kane, *Rev. Mod. Phys.* **82**, 3045 (2010).
- ³X. L. Qi and S. C. Zhang, *Rev. Mod. Phys.* **83**, 1057 (2011).
- ⁴J. E. Moore, *Nature (London)* **464**, 194 (2010).
- ⁵L. Fu, *Phys. Rev. Lett.* **106**, 106802 (2011).
- ⁶R. S. K. Mong, A. M. Essin, and J. E. Moore, *Phys. Rev. B* **81**, 245209 (2010).
- ⁷T. H. Hsieh, H. Lin, J. Liu, W. Duan, A. Bansil, and L. Fu, *Nat. Commun.* **3**, 982 (2012).
- ⁸J. C. Y. Teo, L. Fu, and C. L. Kane, *Phys. Rev. B* **78**, 045426 (2008).
- ⁹Y. Tanaka *et al.*, *Nat. Phys.* **8**, 800 (2012).
- ¹⁰P. Dziawa *et al.*, *Nat. Mater.* **11**, 1023 (2012).
- ¹¹S. Xu *et al.*, *Nat. Commun.* **3**, 1192 (2012).
- ¹²B. M. Wojek *et al.*, *Phys. Rev. B* **87**, 115106 (2013).
- ¹³D. Hsieh *et al.*, *Science* **323**, 919 (2009).
- ¹⁴R. Takahashi and S. Murakami, *Phys. Rev. Lett.* **107**, 166805 (2011).
- ¹⁵H. D. Drew, *Nat. Phys.* **8**, 779 (2012).
- ¹⁶M. Kargarian and G. A. Fiete, *Phys. Rev. Lett.* **110**, 156403 (2013).
- ¹⁷C. Fang, M. J. Gilbert, and B. A. Bernevig, *Phys. Rev. B* **86**, 115112 (2012).
- ¹⁸J. C. Y. Teo and T. L. Hughes, *Phys. Rev. Lett.* **111**, 047006 (2013).
- ¹⁹C.-K. Chiu, H. Yao, and S. Ryu, *Phys. Rev. B* **88**, 075142 (2013).
- ²⁰L. Fu and C. L. Kane, *Phys. Rev. Lett.* **109**, 246605 (2012).
- ²¹R. Buczko and L. Cywinski, *Phys. Rev. B* **85**, 205319 (2012).
- ²²R. Slager, A. Mesaros, V. Juricic, and J. Zaanen, *Nat. Phys.* **9**, 98 (2013).
- ²³P. Jadaun, D. Xiao, Q. Niu, and S. K. Banerjee, *Phys. Rev. B* **88**, 085110 (2013).
- ²⁴D. Khokhlov, *Lead Chalcogenides: Physics and Applications* (CRC Press, Boca Raton, FL, 2002).
- ²⁵G. Bauer and G. Springholz, *Phys. Status Solidi B* **244**, 2752 (2007).
- ²⁶J. Liu, T. Hsieh, W. Duan, J. Moodera, and L. Fu, *Bull. Am. Phys. Soc.*, <http://meetings.aps.org/Meeting/MAR13/Event/185363>.
- ²⁷F. Zhang, C. L. Kane, and E. J. Mele, *Phys. Rev. B* **86**, 081303 (2012).
- ²⁸B. A. Volkov and O. A. Pankratov, *JETP Lett.* **42**, 178 (1985).
- ²⁹V. Korenman and H. D. Drew, *Phys. Rev. B* **35**, 6446 (1987).
- ³⁰E. Fradkin, E. Dagotto, and D. Boyanovsky, *Phys. Rev. Lett.* **57**, 2967 (1986).
- ³¹C. S. Lent, M. A. Bowen, J. D. Dow, R. S. Allgaier, O. F. Sankey, and E. S. Ho, *Superlattices Microstruct.* **2**, 491 (1986).
- ³²S. Safaei, P. Kacman, and R. Buczko, *Phys. Rev. B* **88**, 045305 (2013).
- ³³We performed density functional theory calculations using the generalized gradient approximation (Ref. 34) and the projector augmented wave potential (Ref. 35), as implemented in the Vienna *ab initio* simulation package (Ref. 36).
- ³⁴J. P. Perdew, K. Burke, and M. Ernzerhof, *Phys. Rev. Lett.* **77**, 3865 (1996).
- ³⁵P. E. Blöchl, *Phys. Rev. B* **50**, 17953 (1994).
- ³⁶G. Kresse and J. Furthmüller, *Phys. Rev. B* **54**, 11169 (1996).
- ³⁷C. Fang, M. J. Gilbert, S.-Y. Xu, B. A. Bernevig, and M. Z. Hasan, *Phys. Rev. B* **88**, 125141 (2013).
- ³⁸See Supplemental Material at <http://link.aps.org/supplemental/10.1103/PhysRevB.88.241303> for a discussion of the effects of these additional terms in $k \cdot p$ theory.
- ³⁹Y. J. Wang *et al.*, *Phys. Rev. B* **87**, 235317 (2013).